Programme Area: Carbon Capture and Storage

Project: Storage Appraisal

Title: Pressure Buildup During CO2 Injection into a Closed Brine Aquifer

Abstract:

This document is a supporting document to deliverable MS6.1 UK Storage Appraisal Final Report.

Context:

This £4m project produced the UK's first carbon dioxide storage appraisal database enabling more informed decisions on the economics of CO2 storage opportunities. It was delivered by a consortium of partners from across academia and industry - LR Senergy Limited, BGS, the Scottish Centre for Carbon Storage (University of Edinburgh, Heriot-Watt University), Durham University, GeoPressure Technology Ltd, Geospatial Research Ltd, Imperial College London, RPS Energy and Element Energy Ltd. The outputs were licensed to The Crown Estate and the British Geological Survey (BGS) who have hosted and further developed an online database of mapped UK offshore carbon dioxide storage capacity. This is publically available under the name CO2 Stored. It can be accessed via www.co2stored.co.uk.

APPENDIX A4.1

PRESSURE BUILDUP DURING CO_2 INJECTION INTO A CLOSED BRINE AQUIFER

Simon A. Mathias, Gerardo J. González Martínez de Miguel, Kate E. Thatcher & Robert W. Zimmerman

Transp Porous Med
DOI 10.1007/s11242-011-9776-z

Pressure Buildup During CO_2 Injection into a Closed Brine Aquifer

Simon A. Mathias · Gerardo J. González Martínez de Miguel · Kate E. Thatcher · Robert W. Zimmerman

Received: 24 May 2010 / Accepted: 30 April 2011

Abstract CO_2 injected into porous formations is accommodated by reduction in the volume of the formation fluid and enlargement of the pore space, through compression of the formation fluids and rock material, respectively. A critical issue is how the resulting pressure buildup will affect the mechanical integrity of the host formation and caprock. Building on an existing approximate solution for formations of infinite radial extent, this article presents an explicit approximate solution for estimating pressure buildup due to injection of CO_2 into closed brine aquifers of finite radial extent. The analysis is also applicable for injection into a formation containing multiple wells, in which each well acts as if it were in a quasi-circular closed region. The approximate solution is validated by comparison with vertically averaged results obtained using TOUGH2 with ECO2N (where many of the simplifying assumptions are relaxed), and is shown to be very accurate over wide ranges of the relevant parameter space. The resulting equations for the pressure distribution are explicit, and can be easily implemented within spreadsheet software for estimating CO_2 injection capacity.

Keywords CO_2 injection · Forchheimer's equation · Closed formation · Pressure buildup

S. A. Mathias (✉) · G. J. González Martínez de Miguel · K. E. Thatcher
Department of Earth Sciences, Durham University, Durham, UK
e-mail: s.a.mathias@durham.ac.uk

K. E. Thatcher
e-mail: kate.thatcher@durham.ac.uk

G. J. González Martínez de Miguel
ERC Equipoise Limited, London, UK
e-mail: gerardo@ercequipoise.com

R. W. Zimmerman
Department of Earth Science and Engineering, Imperial College London, London, UK
e-mail: r.w.zimmerman@imperial.ac.uk

Published online: 28 May 2011

List of symbols

A	Formation plan area [L^2]
b	Forchheimer parameter [L^{-1}]
b_r	Relative Forchheimer parameter [-]
c_o	Compressibility of CO_2 [$M^{-1}\,LT^2$]
c_r	Compressibility of geological formation [$M^{-1}\,LT^2$]
c_w	Compressibility of brine [$M^{-1}\,LT^2$]
h	CO_2 brine interface elevation [L]
$h_D = h/H$	Dimensionless interface elevation [-]
H	Formation thickness [L]
k	Permeability [L^2]
k_r	Relative permeability [-]
M_0	Mass injection rate [MT^{-1}]
p	Fluid pressure [$ML^{-1}\,T^{-2}$]
$p_D = 2\pi H\rho_o k_r kp/M_0\mu_o$	Dimensionless pressure [-]
q_o	CO_2 flux [LT^{-1}]
$q_{o\mathrm{D}} = 2\pi Hr_w\rho_o q_o/M_0$	Dimensionless CO_2 flux [-]
q_w	Brine flux [LT^{-1}]
$q_{w\mathrm{D}} = 2\pi Hr_w\rho_o q_w/M_0$	Dimensionless brine flux [-]
r	Radial distance [L]
r_c	Radial extent of reservoir [L]
$r_{cD} = r_c/r_w$	Dimensionless radial extent of reservoir [-]
$r_D = r/r_w$	Dimensionless radius [-]
r_w	Well radius [L]
S_r	Residual brine saturation [-]
t	Time [T]
$t_{cD} = \alpha r_{cD}^2/2.246\gamma$	Dimensionless time at which the pressure disturbance meets the reservoir boundary [-]
$t_D = M_0 t/2\pi(1-S_r)\phi Hr_w^2\rho_o$	Dimensionless time [-]
$\alpha = M_0\mu_o(c_r+c_w)/2\pi(1-S_r)H\rho_o k_r k$	Dimensionless compressibility [-]
$\beta = M_0 k_r k b_r b/2\pi Hr_w\mu_o$	Dimensionless Forchheimer parameter [-]
$\gamma = \mu_o/k_r\mu_w$	Viscosity ratio [-]
$\epsilon = (1-S_r)(c_o-c_w)/(c_r+c_w)$	Normalized fluid compressibility difference [-]
μ_o	Viscosity of CO_2 [$ML^{-1}\,T^{-1}$]
μ_w	Viscosity of brine [$ML^{-1}\,T^{-1}$]
ρ_o	Density of CO_2 [ML^{-3}]
ρ_w	Density of brine [ML^{-3}]
$\sigma = b_r\rho_o/\rho_w$	Density ratio [-]
ϕ	Porosity [-]

1 Introduction

Carbon capture and storage is arguably one of the most promising mitigation technologies currently under consideration to combat CO_2 emission-induced climate change. The process involves capturing CO_2 at the point of generation, compressing it to a supercritical fluid state, and sequestering it at depth within a suitable permeable geological formation. For closed

geological formations, CO_2 injected into a porous formation is accommodated by reduction in the volume of the formation fluid and enlargement of the pore space, through compression of the formation fluids and rock material, respectively. For open formations, injected CO_2 is additionally accommodated by the displacement of native formation fluids from the host formation of concern. A critical concern is how the resulting pressure buildup will affect the mechanical integrity of the host formation and caprock. In assessing the storage capacity of a given formation, one should, therefore, verify that the estimated pressure buildup does not exceed the failure limit of the overlying cap-rock (Mathias et al. 2009a).

The calculation of pressure buildup requires simulating the injection of supercritical CO_2 into the porous formation. This can be achieved using a numerical multi-phase reservoir simulator (e.g., Rutqvist et al. 2008; Birkholzer et al. 2009). However, such models can be expensive to acquire and computationally intensive to run. Therefore, there has been a parallel effort to develop simple semi-analytical methods. The earliest of these assumed Buckley–Leverett displacement (Saripalli and McGrail 2002). The Buckley–Leverett equation describes one-dimensional, two-phase, incompressible, immiscible flow in the absence of capillary pressure (Buckley and Leverett 1942). Nordbotten et al. (2005) took a similar approach by assuming incompressible flow, negligible vertical pressure gradient, and negligible capillary pressure. Their resulting governing equations are mathematically analogous to the Buckley–Leverett equation for the special case when relative permeability is a linear function of fluid saturation. A major advantage of this model is that the saturation distribution can be derived explicitly; a limitation is that calculation of the pressure distribution requires the specification of an arbitrary radius of influence. Zhou et al. (2008) developed an alternative method that accounts for the storage capacity due to formation and fluid compressibility. However, an important limiting assumption in their analysis is that pressure buildup is spatially uniform and independent of formation permeability. More recently, Mathias et al. (2009c) improved on Nordbotten's approach by incorporating formation and fluid compressibility, and developed accurate approximate solutions to the model equations using the method of matched asymptotic expansions. They also proceeded to apply the methodology of Mathias et al. (2008) to obtain a large-time approximation that accounts for inertial effects using the Forchheimer (1901) equation. Inertial effects are particularly important for injection (or production) scenarios, due to the increase in velocity caused by the convergence of flow lines around the injection (or production) well (Mathias et al. 2008; Mathias and Todman 2010).

The analytical solutions of Zhou et al. (2008) and Mathias et al. (2009c) represent two end members of the problem of concern. Zhou's method is useful when the reservoir is small and the permeability is large. Mathias's method, assuming a formation of infinite radial extent, is useful for very large reservoirs where permeability is small. In this article, the approximate solutions of Mathias et al. (2009c) are extended to account for formations of finite radial extent, leading to an approximate analytical solution that is accurate over the entire domain of practical interest. Zhou et al. (2008) additionally account for pressure reduction due to fluid leak-off into the cap-rock. This aspect of Zhou's work is not considered further in this article.

In a recent article, Ehlig-Economides and Economides (2010) extended the heuristic function (inspired by the Buckley–Leverett solution) of Burton et al. (2008) to account for a closed outer boundary of the reservoir formation, by applying a factor of 0.472 to the radius of influence parameter. No explanation was given as to the origin of this factor, but a detailed derivation for the case of single-phase flow can be found in Dake (1978). Although the operational conclusions of Ehlig-Economides and Economides (2010) have received substantial criticism (e.g., Chadwick et al. 2010), their fundamental idea of providing a closed boundary condition is worthy of further consideration. The study in this article can be said to build on

the mathematical development presented by Ehlig-Economides and Economides (2010) in the following respects: (1) a clear derivation is provided concerning the origin of the 0.472 factor in the context of two-phase flow, (2) near-well non-Darcy effects are accounted for using the Forchheimer equation, and (3) the pressure distribution is calculated explicitly without the need for using the Welge (1952) method for tracking the CO_2 front and the heuristic function of Burton et al. (2008) for describing the pressure distribution within the two-phase region.

2 Problem Definition

Following Nordbotten et al. (2005), we assume the existence of a sharp interface located at an elevation, h [L], above the base of the formation, with CO_2 and immobile brine on one side and mobile brine on the other side. Due to CO_2 generally having a lower density than brine, CO_2 is assumed to exist on the upper-side of the interface. We ignore capillary pressure, and assume that the pressure, p [$ML^{-1}T^{-2}$], is in vertical equilibrium over the entire thickness of the confined porous formation of vertical extent H [L]. Saturation, relative permeability, and viscosity are assumed to be constant and uniform within both the CO_2 and the brine zones. In order to obtain a solution for the pressure distribution, the traditional assumption is made that the two fluids and the porous formation each have small compressibilities that do not vary with pressure (Mathias et al. 2009c). Detailed discussions concerning the theoretical basis of these assumptions are presented by Nordbotten et al. (2005), Dentz and Tartakovsky (2009), and Gasda et al. (2009).

From consideration of conservation of mass, the governing equations for the fluid pressure, p, and the interface elevation, h, can be written as

$$(1 - S_r)\frac{\partial}{\partial t}[\phi\rho_o(H - h)] = -\frac{1}{r}\frac{\partial}{\partial r}[r\rho_o(H - h)q_o] \tag{1}$$

$$(1 - S_r)\frac{\partial}{\partial t}(\phi\rho_w h) + S_r H\frac{\partial}{\partial t}(\phi\rho_w) = -\frac{1}{r}\frac{\partial}{\partial r}(r\rho_w h q_w) \tag{2}$$

where the fluxes, q_o [LT^{-1}] and q_w [LT^{-1}], are assumed to be related to pressure gradient by the Forchheimer equation (Forchheimer 1901), as follows:

$$\frac{\mu_o}{k_r k}q_o + b_r b\rho_o q_o|q_o| = -\frac{\partial p}{\partial r} \tag{3}$$

$$\frac{\mu_w}{k}q_w + b\rho_w q_w|q_w| = -\frac{\partial p}{\partial r} \tag{4}$$

where S_r [-] is the residual brine saturation, t [T] is time, ϕ [-] is the porosity, r [L] is the radial distance from the center of the injection well, k [L^2] is absolute permeability, b [L^{-1}] is the Forchheimer parameter, and ρ_o [ML^{-3}], ρ_w [ML^{-3}], μ_o [$ML^{-1}T^{-1}$], and μ_w [$ML^{-1}T^{-1}$] are the densities and viscosities of the CO_2 and brine, respectively. The factors k_r [-] and b_r [-] are the relative permeability and relative Forchheimer parameters, respectively, for the CO_2, representing the fact that the transmissivity of the CO_2 is reduced due to the presence of the residual brine saturation, S_r (see Bennion and Bachu 2008). Relative permeability and relative Forchheimer parameters for the brine are not required in this article, because the brine saturation is assumed to be 1 before it is displaced by CO_2.

The problem under consideration is constrained by the following initial and boundary conditions:

$$\begin{array}{lll} p = 0, & r \geq 0, & t = 0 \\ h = H, & r \geq 0, & t = 0 \\ q_o = M_0/(2\pi H \rho_o r_w), & r = r_w, & t > 0 \\ q_o = 0, & r = r_c, & t > 0 \\ q_w = 0, & r = r_w, & t > 0 \\ q_w = 0, & r = r_c, & t > 0 \end{array} \tag{5}$$

where M_0 [MT^{-1}] is the mass injection rate, r_w [L] is the well radius, and r_c [L] is the outer radius of the formation.

Substituting the compressibilities for the geological formation, CO_2 and brine $c_r = \phi^{-1}(\mathrm{d}\phi/\mathrm{d}p)$ [$\mathrm{M}^{-1}\,\mathrm{LT}^2$], $c_o = \rho_o^{-1}(\mathrm{d}\rho_o/\mathrm{d}p)$ [$\mathrm{M}^{-1}\,\mathrm{LT}^2$], and $c_w = \rho_w^{-1}(\mathrm{d}\rho_w/\mathrm{d}p)$ [$\mathrm{M}^{-1}\,\mathrm{LT}^2$], respectively (Bear 1979), then leads to

$$(1 - S_r)\phi\rho_o \left[(c_r + c_o)(H - h)\frac{\partial p}{\partial t} - \frac{\partial h}{\partial t} \right] = -\frac{1}{r}\frac{\partial}{\partial r}[r\rho_o(H - h)q_o] \tag{6}$$

$$(1 - S_r)\phi\rho_w \left[(c_r + c_w)\left(\frac{S_r H}{(1 - S_r)} + h \right)\frac{\partial p}{\partial t} + \frac{\partial h}{\partial t} \right] = -\frac{1}{r}\frac{\partial}{\partial r}(r\rho_w h q_w) \tag{7}$$

Making the usual assumption that the fluid and formation compressibilities, c_r, c_o, c_w, are small, it follows that the porosity, ϕ, and the densities, ρ_o and ρ_w, can be treated as constant, in which case Eqs. 6 and 7 simplify to

$$(1 - S_r)\phi(c_r + c_w)\left[\frac{H}{1 - S_r} + \left(\frac{c_o - c_w}{c_r + c_w} \right)(H - h) \right]\frac{\partial p}{\partial t} = -\frac{1}{r}\frac{\partial}{\partial r}\{r[(H - h)q_o + hq_w]\} \tag{8}$$

$$(1 - S_r)\phi\frac{\partial h}{\partial t} = -\frac{1}{r}\frac{\partial}{\partial r}(rhq_w) - \phi(c_r + c_w)\left[S_r H + (1 - S_r)h\right]\frac{\partial p}{\partial t} \tag{9}$$

The analysis of this problem can be further simplified by consideration of the following dimensionless groups (Mathias et al. 2009c):

$$r_D = \frac{r}{r_w}, \quad r_{cD} = \frac{r}{r_c}, \quad t_D = \frac{M_0 t}{2\pi(1 - S_r)\phi H r_w^2 \rho_o} \tag{10}$$

$$q_{o\mathrm{D}} = \frac{2\pi H r_w \rho_o q_o}{M_0}, \quad q_{w\mathrm{D}} = \frac{2\pi H r_w \rho_o q_w}{M_0} \tag{11}$$

$$p_D = \frac{2\pi H \rho_o k_r k p}{M_0 \mu_o}, \quad h_D = \frac{h}{H} \tag{12}$$

$$\alpha = \frac{M_0 \mu_o (c_r + c_w)}{2\pi(1 - S_r)H\rho_o k_r k}, \quad \beta = \frac{M_0 k_r k b_r b}{2\pi H r_w \mu_o}, \quad \gamma = \frac{\mu_o}{k_r \mu_w} \tag{13}$$

$$\epsilon = (1 - S_r)\frac{c_o - c_w}{c_r + c_w}, \quad \sigma = \frac{b_r \rho_o}{\rho_w} \tag{14}$$

such that the problem can be written in terms of dimensionless variables as follows:

$$[1 + \epsilon(1 - h_D)]\,\alpha\frac{\partial p_D}{\partial t_D} = -\frac{1}{r_D}\frac{\partial}{\partial r_D}\{r_D\left[(1 - h_D)\,q_{o\mathrm{D}} + h_D q_{w\mathrm{D}}\right]\} \tag{15}$$

$$\frac{\partial h_D}{\partial t_D} = -\frac{1}{r_D}\frac{\partial}{\partial r_D}(r_D h_D q_{w\mathrm{D}}) - \alpha[S_r + (1 - S_r)h_D]\frac{\partial p_D}{\partial t_D} \tag{16}$$

$$q_{o\mathrm{D}} + \beta q_{o\mathrm{D}} |q_{o\mathrm{D}}| = -\frac{\partial p_D}{\partial r_D} \tag{17}$$

$$q_{w\mathrm{D}} + \frac{\gamma\beta}{\sigma} q_{w\mathrm{D}} |q_{w\mathrm{D}}| = -\gamma \frac{\partial p_D}{\partial r_D} \tag{18}$$

$$\begin{array}{llll} p_D = 0, & r_D \geq 0, & t_D = 0 \\ h_D = 1, & r_D \geq 0, & t_D = 0 \\ q_{o\mathrm{D}} = 1, & r_D = 1, & t_D > 0 \\ q_{o\mathrm{D}} = 0, & r_D = r_{cD}, & t_D > 0 \\ q_{w\mathrm{D}} = 0, & r_D = 1, & t_D > 0 \\ q_{w\mathrm{D}} = 0, & r_D = r_{cD}, & t_D > 0 \end{array} \tag{19}$$

3 Solution for Domain of Infinite Extent

Previously, it has been shown that when $r_{cD} \to \infty, r_{wD} \to 0, \epsilon \to 0, t_D \gg \beta^2/2\gamma$ and $\alpha \ll 1$ (Mathias et al. 2009c),

$$p_D \approx \begin{cases} F_D(2/\gamma, t_D) - \dfrac{1}{2} \ln\left(\dfrac{x}{2\gamma}\right) - 1 + \dfrac{1}{\gamma} + \dfrac{\beta}{(xt_D)^{1/2}}, & x \leq 2\gamma \\ F_D(2/\gamma, t_D) - \left(\dfrac{x}{2\gamma}\right)^{1/2} + \dfrac{1}{\gamma}, & 2\gamma < x < 2/\gamma \\ F_D(x, t_D), & x \geq 2/\gamma \end{cases} \tag{20}$$

where

$$F_D(x, t_D) = \frac{1}{2\gamma} E_1\left(\frac{\alpha x}{4\gamma}\right) \approx -\frac{1}{2\gamma} \ln\left(\frac{\alpha x}{2.246\gamma}\right) \tag{21}$$

where $x = r_D^2/t_D$ and E_1 denote the En function with $n = 1$, which is related to the exponential integral function, $Ei(x)$, via $E_1(x) = -Ei(-x)$. The range $2\gamma < x < 2/\gamma$ contains the region where mobile brine and CO_2 co-exist.

The Thiem equation for steady-state single-phase radial flow of a fluid of density, ρ_o, and viscosity, μ_w, in a formation with a radius of influence r_e [L], can be written as (also see Dake 1978, p. 139)

$$p = \frac{M_0 \mu_w}{2\pi\rho_o k H} \ln\left(\frac{r_e}{r}\right) \tag{22}$$

Applying the dimensionless transformations and setting $p_D = F_D$ leads to

$$F_D(x, t_D) = -\frac{1}{2\gamma} \ln\left(\frac{r_D^2}{r_{eD}^2}\right) \tag{23}$$

where $r_{eD} = r_e/r_w$.

Equating Eqs. 21 and 23, it follows that

$$\frac{t_D}{r_{eD}^2} = \frac{\alpha}{2.246\gamma} \tag{24}$$

It can be said that the pressure perturbation has reached the boundary when $r_e = r_c$. From this, it can be inferred that Eq. 20 in conjunction with Eq. 21 is also valid for formations of finite extent, provided that $t_D < t_{cD}$ where

$$t_{cD} = \frac{\alpha r_{cD}^2}{2.246\gamma} \tag{25}$$

4 Quasi-Static Solution for Single-Phase Flow

Now consider radial single-phase flow of a fluid of density, ρ_o, and viscosity, μ_w, in a closed formation of outer radius, r_c. The governing conservation equation for flow from a fully penetrating well in a homogeneous, isotropic, and confined aquifer is

$$\phi(c_r + c_w)\frac{\partial p}{\partial t} = -\frac{1}{r}\frac{\partial}{\partial r}(rq_w) \tag{26}$$

where the flux q_w [LT^{-1}] is found from Darcy's law,

$$q_w = -\frac{k}{\mu_w}\frac{\mathrm{d}p}{\mathrm{d}r} \tag{27}$$

The relevant initial and boundary conditions are:

$$\begin{array}{lll} p = 0, & r_i \le r \le r_c, & t = 0 \\ q_w = M_0/(2\pi\rho_o r_i H), & r = r_i, & t > 0 \\ q_w = 0, & r = r_c, & t > 0 \end{array} \tag{28}$$

where r_i [L] is the radius of another injection well.

After sufficient time has passed for $r_e > r_c$, the change in pressure with time becomes more or less uniform, making the right-hand-side of Eq. 26 a constant. To determine the value of that constant we can write

$$\frac{\mathrm{d}p}{\mathrm{d}t} \approx \frac{\mathrm{d}p}{\mathrm{d}V}\frac{\mathrm{d}V}{\mathrm{d}t} = \left(\frac{1}{V}\frac{\mathrm{d}V}{\mathrm{d}p}\right)^{-1}\frac{1}{V}\frac{\mathrm{d}V}{\mathrm{d}t} \tag{29}$$

where $V = AH\phi$ [L^3] is the volume of fluid in the reservoir, $A = \pi(r_c^2 - r_i^2)$ [L^2] is the plan area of the reservoir, $V^{-1}\mathrm{d}V/\mathrm{d}p = c_w + c_r$ [$M^{-1}LT^2$] and $\mathrm{d}V/\mathrm{d}t = M_0/\rho_o$ [L^3T^{-1}] such that

$$\frac{\mathrm{d}p}{\mathrm{d}t} \approx \frac{M_0}{\rho_o AH\phi(c_w + c_r)} \tag{30}$$

which on integration yields an estimate of the mean pressure

$$\overline{p} \approx \frac{M_0 t}{\rho_o AH\phi(c_w + c_r)} \tag{31}$$

With the assumption that $\mathrm{d}p/\mathrm{d}t$ is a constant, we can also write Eq. 26 as an ordinary differential equation with r as the independent variable:

$$\frac{M_0}{\rho_o AH} \approx -\frac{1}{r}\frac{\mathrm{d}}{\mathrm{d}r}(rq_w) \tag{32}$$

which on integration and imposing the no-flow boundary at $r = r_c$ yields

$$q_w = -\frac{M_0}{2\rho_o AH}\left(r - \frac{r_c^2}{r}\right) \tag{33}$$

Substitution into Darcy's law gives

$$\frac{\mathrm{d}p}{\mathrm{d}r} = \frac{M_0\mu_w}{2\rho_o kAH}\left(r - \frac{r_c^2}{r}\right) \tag{34}$$

Integrating again and setting $p = p_i$ at $r = r_i$ gives

$$p - p_i = \frac{M_0\mu_w}{2\rho_o kAH}\left[\frac{r^2 - r_i^2}{2} - r_c^2 \ln\left(\frac{r}{r_i}\right)\right] \tag{35}$$

The mean pressure is obtained by integration, as follows:

$$\overline{p} - p_i = \frac{2\pi}{A}\int_{r_i}^{r_c} r(p - p_i)\,\mathrm{d}r = \frac{\pi M_0\mu_w}{2\rho_o kA^2H}\left[\frac{3r_c^4}{4} - r_c^2 r_i^2 + \frac{r_i^4}{4} - r_c^4 \ln\left(\frac{r_c}{r_i}\right)\right] \tag{36}$$

Assuming that $r_c \gg r_i$, $A \approx \pi r_c^2$ and $\overline{p} \approx M_0 t/[\pi\rho_o r_c^2 H\phi(c_r + c_w)]$, so (Dake 1978, p. 139)

$$p_i = \frac{M_0 t}{\pi\rho_o r_c^2 H\phi(c_r + c_w)} - \frac{M_0\mu_w}{2\pi\rho_o kH}\left[\frac{3}{4} - \ln\left(\frac{r_c}{r_i}\right)\right] \tag{37}$$

5 Incorporation Within the Two-phase Solution

We now set r_i as the outside edge of the two-phase region. Recalling that $x = (r/r_w)^2/t_D$, and that the outside edge of the two-phase region is defined by $x = 2/\gamma$, it follows that $(r_i/r_w)^2/t_D = 2/\gamma$, and $r/r_i = (\gamma x/2)^{1/2}$. Assuming that the pressure distribution in the far-field region obeys Eq. 35 (i.e., $F_D(2/\gamma, t_D) = p_{iD}$), Eq. 20 can be rewritten as

$$p_D - p_{iD} \approx \begin{cases} -\ln\left(\dfrac{r}{\gamma r_i}\right) - 1 + \dfrac{1}{\gamma} + \dfrac{\beta r_w}{r}, & r_w \le r \le \gamma r_i \\ -\dfrac{r}{\gamma r_i} + \dfrac{1}{\gamma}, & \gamma r_i < r < r_i \\ \dfrac{\pi r_c^2}{\gamma A}\left[\dfrac{r^2 - r_i^2}{2r_c^2} - \ln\left(\dfrac{r}{r_i}\right)\right], & r_i \le r \le r_c \end{cases} \tag{38}$$

where $p_{iD} = 2\pi H\rho_o k_r k p_i/M_0\mu_o$.

The mean dimensionless pressure is defined by

$$\overline{p}_D - p_{iD} = \frac{2\pi}{A}\int_{r_w}^{r_c} r(p_D - p_{iD})\,\mathrm{d}r \tag{39}$$

which can be integrated to yield

$$p_{iD} = \frac{2\pi r_w^2 t_D}{\alpha A} - \frac{2\pi}{A}\left\{\beta(\gamma r_i r_w - r_w^2) + \left(1 + \frac{2}{\gamma^3}\right)\frac{\gamma^2 r_i^2}{12} - \left[\ln\left(\frac{\gamma r_i}{r_w}\right) - \frac{1}{2} + \frac{1}{\gamma}\right]\frac{r_w^2}{2} + \left[\frac{3}{4} - \ln\left(\frac{r_c}{r_i}\right) - \frac{r_i^2}{r_c^2} + \frac{r_i^4}{4r_c^4}\right]\frac{\pi r_c^4}{2\gamma A}\right\} \tag{40}$$

Recall from Eq. 31 that $\overline{p} \approx M_0 t/[\pi \rho_o r_c^2 H \phi (c_r + c_w)]$.

From the above, it can be said that the analogue of Eq. 21 for a closed formation is

$$F_D(x, t_D) = \begin{cases} \dfrac{1}{2\gamma} E_1\left(\dfrac{\alpha x}{4\gamma}\right), & t_D < t_{cD} \\ p_{iD} + \dfrac{\pi r_c^2}{A}\left[\dfrac{(\gamma x - 2)t_D}{2\gamma^2 r_{cD}^2} - \dfrac{1}{2\gamma}\ln\left(\dfrac{\gamma x}{2}\right)\right], & t_D > t_{cD} \end{cases} \tag{41}$$

where t_{cD} is found from Eq. 25. Assuming that $r_c \gg r_i$ (i.e., the radial extent of the CO_2 plume is always much smaller than that of the formation), $A = \pi r_c^2$, and the above solution reduces to

$$F_D(x, t_D) \approx \begin{cases} \dfrac{1}{2\gamma} E_1\left(\dfrac{\alpha x}{4\gamma}\right), & t_D < t_{cD} \\ \dfrac{2t_D}{\alpha r_{cD}^2} - \dfrac{1}{\gamma}\left[\dfrac{3}{4} - \dfrac{1}{2}\ln\left(\dfrac{r_{cD}^2}{x t_D}\right) - \dfrac{(\gamma x - 2)t_D}{2\gamma r_{cD}^2}\right], & t_D > t_{cD} \end{cases} \tag{42}$$

So the semi-analytical solution of Mathias et al. (2009c) (i.e., Eqs. 20 and 21) can be extended to deal with closed formations by replacing Eq. 21 with Eq. 42. Note that $3/4 = -\ln(0.472)$, which explains the origin of the factor 0.472 that appears in Ehlig-Economides and Economides (2010).

6 Comparison with TOUGH2 ECO2N

The derivation of the approximate solution given by Eqs. 20 and 42 involves the application of a number of simplifying assumptions, among which the most important are: (1) vertical pressure equilibrium; (2) negligible capillary pressure; (3) constant fluid properties; and (4) immiscible displacement. To assess the impact of these assumptions, the approximate solution is now compared to simulations conducted with the reservoir simulator TOUGH2 (Pruess et al. 1999) using the CO_2 and brine equations of state stored in the ECO2N module (Pruess 2005). The scenarios simulated were loosely based on those previously described by Zhou et al. (2008).

The TOUGH2 simulations assume a fully penetrating well situated at the origin of a two-dimensional radially symmetric closed flow-field. The model assumes the van Genuchten (1980) relationship between brine effective saturation, S_e [-], and capillary pressure, P_c [$ML^{-1}T^{-2}$]

$$S_e = \left(1 + \left|\frac{P_c}{P_{c,0}}\right|^n\right)^{-m}, \quad n = \frac{1}{1-m} \tag{43}$$

and that brine and CO_2 relative permeability are linearly related to S_e and $(1 - S_e)$, respectively. In the absence of residual CO_2 saturation, the effective brine saturation is defined by $S_e = (S_w - S_r)/(1 - S_r)$, where S_w [-] is the total brine saturation (the volumetric proportion of pore-space occupied by brine) and S_r [-] is the residual brine saturation.

The model parameters used were as follows:

Area, $A = 1257\,\text{km}^2$
Radial extent, $r_c = 20\,\text{km}$

Porosity, $\phi = 0.2$
Residual brine saturation, $S_r = 0.5$
End-point relative permeability for CO_2, $k_r = 0.3$
Well radius, $r_w = 0.2$ m
Rock compressibility, $c_r = 4.5 \times 10^{-10}\,\mathrm{Pa}^{-1}$
Forchheimer parameter, $b = 0$
Injection rate, $M_0 = 100$ kg/s
Initial pressure, $P_0 = 10$ MPa
Temperature, $T = 40$°C
Salinity, $S = 0.15$ kg/l
van Genuchten parameter, $m = 0.46$
van Genuchten parameter, $P_{c0} = 19600$ Pa
Formation thickness, $H = 50$ or 200 m
Permeability, $k = 10^{-13}$ or $10^{-12}\,\mathrm{m}^2$

Vertically, the domain was divided into ten equally spaced layers, which corresponds to 5 m/layer in the case of a 50-m thickness aquifer and 20 m/layer in the case of a 200-m thickness aquifer. To invoke a mean initial pressure of 10 MPa, the initial pressure distribution was set to impose initially hydrostatic conditions with pressure along the central horizontal axis set at 10 MPa. Horizontally, the 20- km radial extent of the model was divided into four sub-domains with boundaries located at 0.2, 10, 500, 1000, and 20,000 m from the origin. Each sub-domain was discretized in the radial direction by a set of logarithmically spaced nodes. The inner zone contained two-hundred nodes, the outer zone contained fifty nodes, and the two intermediate zones contained one-hundred nodes each. The four zones were necessary to allow sufficiently high resolution around the well without requiring an excessive number of grid-points. Specifically, the four sub-domains allowed the node spacing to grow from 5 mm at the well-face to 3280 m at the outer boundary using only 450 nodes in the radial direction. Such refinement was found to be necessary to ensure adequate resolution for accurately evaluating well pressures.

Vertically averaged (by taking the mean in the vertical direction) well pressures from the TOUGH2 ECO2N two-dimensional miscible radial flow simulations are presented in Fig. 1 as green thick lines (2D Miscible). For the case presented in Fig. 1d ($k = 10^{-12}\,\mathrm{m}^2$ and $H = 200$ m), the TOUGH2 simulation was terminated after just less than a year due to model convergence difficulties. Nevertheless, all four scenarios exhibit a similar pressure response. Pressure increases monotonically with time. After 10^{-6} years, the pressure increase exhibits a constant linear-log slope until around 10^{-4} years beyond which pressure increases according to a new reduced linear-log slope. The latter effect is due to an increase in CO_2 relative permeability that develops once the residual brine is evaporated in the near-well region. Finally, after around 10 years, the pressure disturbance reaches the outer boundary of the reservoir and the well pressure increases asymptotically.

Plotted alongside, as black dashed lines (Approx. Sol. 1), are well pressures estimated using the approximate solution with fluid properties calculated for the initial pressure using equations previously presented by Mathias et al. (2009a,b). Approx. Sol. 1 shows the correct initial linear-log slope, but tends to overestimate the pressure buildup and does not predict the reduction in slope due to brine evaporation. Nevertheless, Approx. Sol. 1 predicts similar (to TOUGH2) pressure increases once the pressure wave reaches the outer boundary.

To explore the role of gravity in pressure evolution, the TOUGH2 simulations were repeated but with just one layer for the entire formation thickness (as opposed to ten). Well pressures for these are plotted in Fig. 1 as thin black lines (1D Miscible). It is clear that there

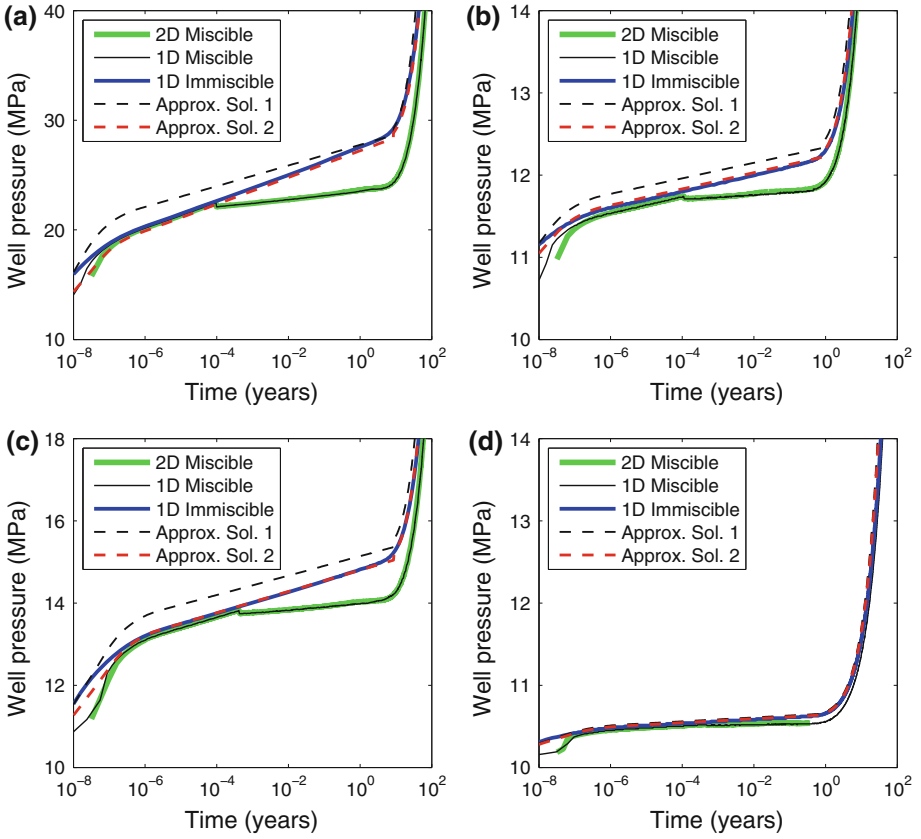

Fig. 1 Comparison of well pressures from the approximate solution with output from TOUGH2 ECO2N (2D Miscible, 1D Miscible, and 1D Immiscible). The output from 2D Miscible is vertically averaged by taking the mean in the vertical direction. Approx. Sol. 1 uses fluid properties based on the initial pressure. Approx. Sol. 2 uses fluid properties based on the pressure given by Approx. Sol. 1 at $t_D = t_{cD}$. **a** $k = 10^{-13}\,\mathrm{m}^2$ and $H = 50\,\mathrm{m}$, **b** $k = 10^{-12}\,\mathrm{m}^2$ and $H = 50\,\mathrm{m}$, **c** $k = 10^{-13}\,\mathrm{m}^2$ and $H = 200\,\mathrm{m}$, and **d** $k = 10^{-12}\,\mathrm{m}^2$ and $H = 200\,\mathrm{m}$

is very little difference between vertically averaged well pressures estimated by 2D Miscible and 1D Miscible, from which it is concluded that gravity has little impact on vertically averaged well pressures for these scenarios.

To explore the role of miscibility (evaporation of brine and dissolution of CO_2), the one-dimensional TOUGH2 simulations were repeated with the solubility limits of CO_2 in brine and water in CO_2 set to zero. Well pressures for these are plotted in Fig. 1 as thick blue lines (1D Immiscible). The pressure response for 1D Immiscible closely follows that for 2D Miscible except that 1D Immiscible maintains the initial linear-log slope until the pressure wave hits the reservoir boundary. This is because brine is not evaporated and the presence of residual brine is maintained around the well-bore throughout the simulation. Approx. Sol. 1 (black dashed lines) closely mimics the 1D Immiscible results although it consistently overestimates pressure due to the assumption of a constant CO_2 fluid density based on the initial pressure.

Vilarrasa et al. (2010) attempted to address this problem by iterating their analytical solution until the resulting mean pressure is equal to the pressure assumed for calculating the fluid

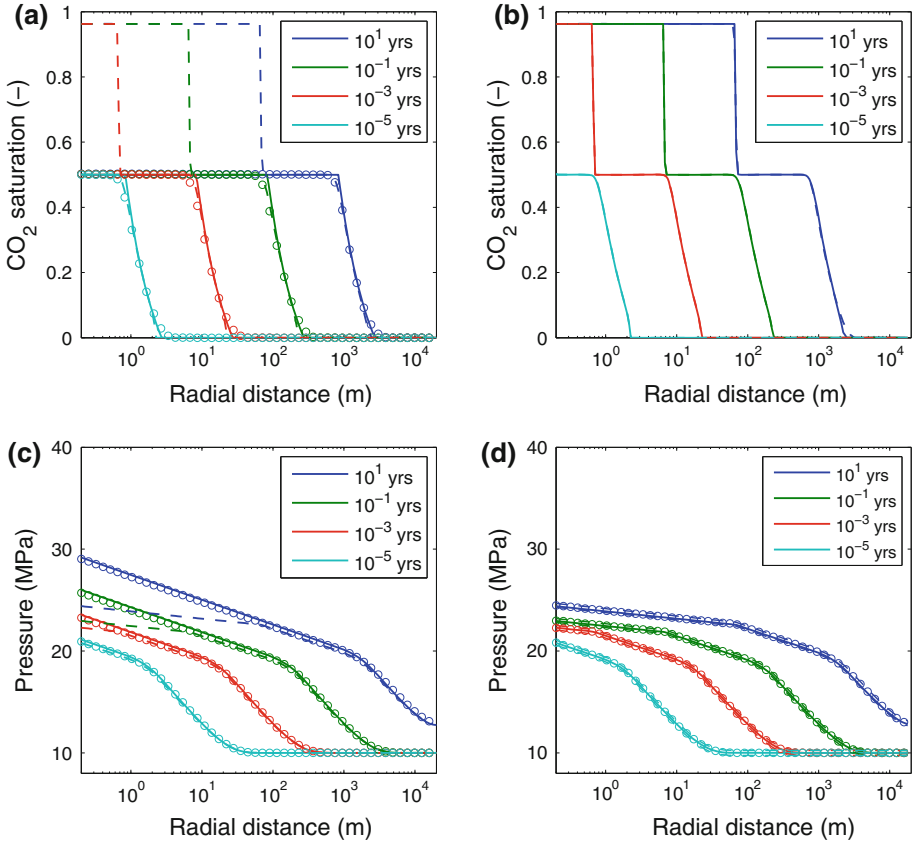

Fig. 2 Profile plots for $k = 10^{-13}\text{m}^2$ and $H = 50\,\text{m}$ (i.e., the scenario assumed for Fig. 1a). **a** and **c** saturation and pressure profiles, respectively, obtained from Approx. Sol. 2 (*solid lines*) compared with corresponding output from 1D Miscible (*dashed lines*) and 1D Immiscible (*circular markers*) simulations from TOUGH2 ECO2N. **b** and **d** saturation and pressure profiles, respectively, obtained from 1D Miscible TOUGH2 ECO2N simulations (*solid lines*) and 2D Miscible TOUGH2 ECO2N simulations (*dashed lines*). In **d** there are two *dashed lines* for each 2D Miscible profile; the *lower* and *upper lines* are for pressures at the top and bottom of the formation, respectively. The *circular markers* are vertically averaged pressures from 2D Miscible

properties. We use a simpler method, which involves re-evaluating the approximate solution using a second set of fluid properties based on the well pressure (from the first iteration) that occurs when the pressure disturbance meets the outer boundary of the reservoir (i.e., $t_D = t_{cD}$). The basis for choosing this pressure is that one is unlikely to want to inject fluid far beyond this point, as the fracture pressure is quickly approached once the outer boundary is felt. The resulting set of curves are the thicker red dashed lines (Approx. Sol. 2) in Fig. 1. Once the pressure for calculating the fluid properties is corrected in this way, the approximate solution can be seen to accurately approximate 1D Immiscible for each of the four scenarios studied.

Recalling that there is negligible difference between vertically averaged well pressures estimated by 2D Miscible and 1D Miscible, the above discussion leads empirically to the conclusion that (1) vertical pressure equilibrium; (2) negligible capillary pressure; and (3) constant fluid properties; are useful assumptions for estimating vertically averaged well

pressures. However, the assumption of immiscible displacement leads to an overestimate of pressure buildup during intermediate times due to the ignoring of brine evaporation around the well-bore.

Although well pressure is of primary interest in this context (Mathias et al. 2009a), it is interesting to study the spatial distributions of pressure and CO_2 predicted by the approximate solution as well. Figure 2a and c presents saturation and pressure profiles, respectively, at various times for the case presented in Fig. 1a ($k = 10^{-13}\text{m}^2$ and $H = 50$ m) as predicted by 1D Miscible, 1D Immiscible, and Approx. Sol. 2 (saturation profiles are obtained using Eq. 26 of Mathias et al. 2009c). The saturation and pressure profiles for 1D Immiscible and Approx. Sol. 2 are virtually identical. These are also very similar to those for 1D Miscible, outside the dry-out zone (where CO_2 saturation rises above $(1 - S_r)$ around the well-bore). Inside the dry-out zone, 1D Miscible predicts lower pressure gradients due to

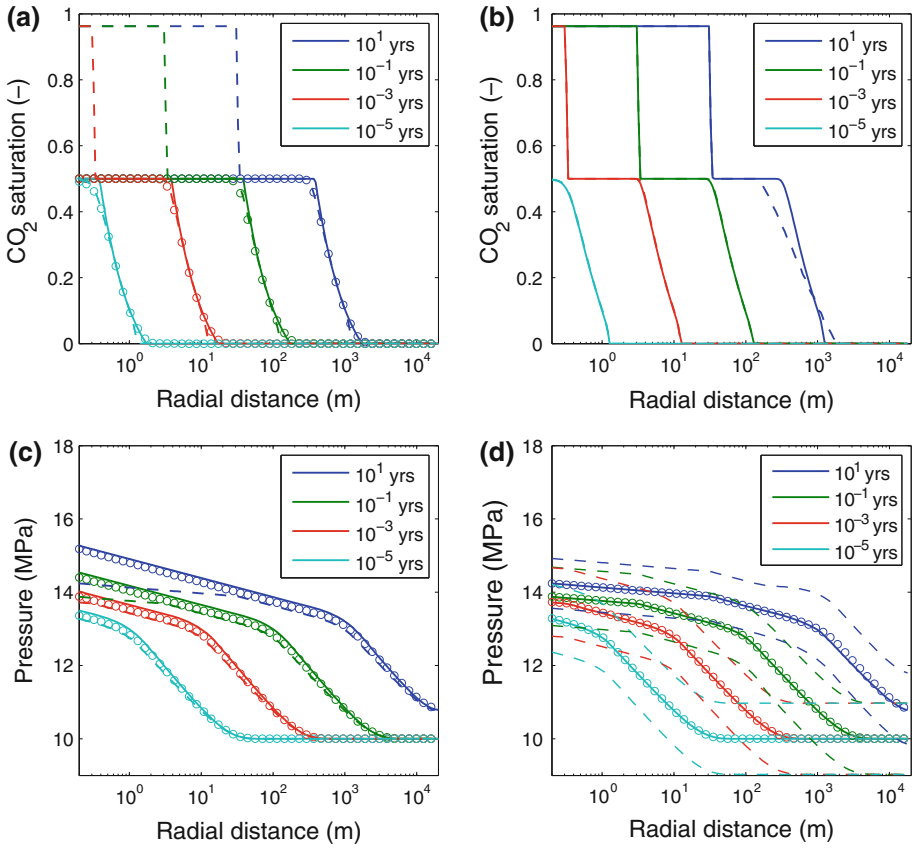

Fig. 3 Profile plots for $k = 10^{-13}\text{m}^2$ and $H = 200$ m (i.e., the scenario assumed for Fig. 1c). **a** and **c** saturation and pressure profiles, respectively, obtained from Approx. Sol. 2 (*solid lines*) compared with corresponding output from 1D Miscible (*dashed lines*) and 1D Immiscible (*circular markers*) simulations from TOUGH2 ECO2N. **b** and **d** saturation and pressure profiles, respectively, obtained from 1D Miscible TOUGH2 ECO2N simulations (*solid lines*) and 2D Miscible TOUGH2 ECO2N simulations (*dashed lines*). In **d** there are *two dashed lines* for each 2D Miscible profile; the *lower* and *upper lines* are for pressures at the top and bottom of the formation, respectively. The *circular markers* are vertically averaged pressures from 2D Miscible

the increased availability of permeable pathways for CO_2 resulting from the evaporation of the residual brine.

Figure 2b compares 1D Miscible with vertically averaged (by taking the mean in the vertical direction) CO_2 saturations from 2D Miscible. Figure 2d compares 1D Miscible with bottom (upper dashed line), top (lower dashed line), and vertically averaged pressures (circular markers) from 2D Miscible. There is negligible difference between results from 1D Miscible and 2D Miscible again verifying that the vertical equilibrium assumption is highly appropriate for this scenario.

However, the $k = 10^{-13}\text{m}^2$ and $H = 50\,\text{m}$ scenario is least likely to be effected by gravity segregation due it having the smallest permeability and smallest formation thickness. Figure 3 shows the same data as Fig. 2 but for the case presented in Fig. 1c ($k = 10^{-13}\text{m}^2$ and $H = 200\,\text{m}$). Again, Fig. 3a and c demonstrate the ability of Approx. Sol. 2 to accurately approximate the internal states of 1D Immiscible. However, in Fig. 3b it is seen that for times > 0.1 years, there is a significant difference between the vertically averaged CO_2 saturation from 2D Miscible and that of 1D Miscible. This is due to the effect of gravity segregation (Lu et al. 2009; Yamamoto and Doughty 2011). Figure 3d compares pressures estimated by 1D Miscible and 2D Miscible. Although there is a wide variation between the upper and lower pressures (the dashed lines), 1D Miscible again provides an accurate estimate of vertically averaged pressure (the circular markers). The variations between the upper and lower pressures are largely due to differences in elevation. Total hydrostatic pressure over the reservoir formation is ($\rho_w g H =$) 0.54 MPa when $H = 50$ m and 2.17 MPa when $H = 200$ m.

7 Summary and Conclusions

When seeking to estimate storage capacity of geological reservoirs for CO_2 geo-sequestration, it is necessary to be able to estimate the pressure buildup resulting from the injection process. Previously, Mathias et al. (2009c) derived a semi-analytical solution for predicting pressure buildup when the formation can be assumed to be of infinite radial extent. In this article, the study of Mathias et al. (2009c) is extended to account for finite outer boundaries, by invoking a quasi-static condition. The semi-analytical solution was verified by comparison with vertically averaged results from TOUGH2 simulations of the fully dynamic problem. This study also shows how to modify the solution presented in Mathias et al. (2009c), to account for residual brine saturation and the associated reduction in the effective relative permeability of the CO_2. The resulting equations remain simple to evaluate in spreadsheet software, and can be easily implemented in currently available storage capacity estimation frameworks (e.g., Mathias et al. 2009a).

Acknowledgments This study was partially funded by the UK Energy Technology Institute's (ETI) UK Storage Appraisal Project (UKSAP) and funding from both the UK Natural Environment Research Council (NERC) and the UK Technology Strategy Board (TSB) provided through the UK Knowledge Transfer Partnership (KTP) scheme.

References

Bear, J.: Hydraulics of Groundwater. McGraw-Hill, New York (1979)

Bennion, D.B., Bachu, S.: Drainage and imbibition relative permeability relationships for supercritical CO_2/brine and H_2S/brine systems in intergranular sandstone, carbonate, shale, and annhydrite rocks. SPE Reserv. Eval. Eng. June, 487–496 (2008)

Birkholzer, J.T., Zhou, Q., Tsang, C.F.: Large-scale impact of CO_2 storage in deep saline aquifers: A sensitivity study on pressure response in stratified systems. Int. J. Greenhouse Gas Control **3**, 181–194 (2009). doi:10.1016/j.ijggc.2008.08.002

Buckley, S.E., Leverett, M.C.: Mechanism of fluid displacement in sands. Trans. Am. Inst. Min. Metall. Pet. Eng. **146**, 107–116 (1942)

Burton, M., Kumar, N., Bryant, S.L.: Time-dependent injectvity during co_2 storage in aquifers. In: SPE/DOE Improved Oil Recovery Symposium held in Tulsa, Oklahoma, USA, 19–23 April (2008). SPE 113937

Chadwick, A., Hodrien, C., Hovorka, S., Mackay, E., Mathias, S., Lovell, B., Kalaydjian, F., Sweeney, G., Benson, S., Dooley, J., Davidson, C.: The realities of storing carbon dioxide—a response to CO_2 storage capacity issues raised by Ehlig-Economides & Economides. Technical report, Published by the European Technology Platform for Zero Emission Fossil Fuel Power Plants (ZEP) (2010). doi:10.1038/npre.2010.4500.1

Dake, L.P.: Fundamentals of Reservoir Engineering. 17th Impression. Elsevier, Amsterdam (1978)

Dentz, M., Tartakovsky, D.M.: Abrupt-interface solution for carbon dioxide injection into porous media. Transp. Porous Media **79**, 15–27 (2009). doi:10.1007/s11242-008-9268-y

Ehlig-Economides, C.A., Economides, M.J.: Sequestering carbon dioxide in a closed underground volume. J. Pet. Sci. Eng. **70**, 123–130 (2010). doi:10.1016/j.petrol.2009.11.002

Forchheimer, P.: Wasserbewegung durch Boden. Z. Ver. Dtsch. Ing **45**, 1782–1788 (1901)

Gasda, S., Nordbotten, J.M., Celia, M.A.: Vertical equilibrium with sub-scale analytical methods for geological CO_2 sequestration. Comput. Geosci. **13**(4), 469–481 (2009). doi:10.1007/s10596-009-9138-x

Lu, C., Lee, S.Y., Han, W.S., McPherson, B.J., Lichtner, P.C.: Comments on "abrupt-interface solution for carbon dioxide injection into porous media" by M. Dentz and D. Tartakovsky. Transp. Porous Media **79**, 29–37 (2009). doi:10.1007/s11242-009-9362-9

Mathias, S.A., Todman, L.C.: Step-drawdown tests and the Forchheimer equation. Water Resour. Res. **46**, W07514 (2010). doi:10.1029/2009WR008635

Mathias, S.A., Butler, A.P., Zhan, H.: Approximate solutions for Forchheimer flow to a well. J. Hydraul. Eng. **134**(9), 1318–1325 (2008). doi:10.1061/(ASCE)0733-9429(2008)134:9(1318)

Mathias, S.A., Hardisty, P.E., Trudell, M.R., Zimmerman, R.W.: Screening and selection of sites for CO_2 sequestration based on pressure buildup. Int. J. Greenhouse Gas Control **3**, 577–585 (2009a). doi:10.1016/j.ijggc.2009.05.002

Mathias, S.A., Hardisty, P.E., Trudell, M.R., Zimmerman, R.W.: Erratum to screening and selection of sites for CO_2 sequestration based on pressure buildup [Int. J. Greenhouse Gas Control **3**(5) (2009) 577–585]. Int. J. Greenhouse Gas Control **4**, 108–109 (2009b). doi:10.1016/j.ijggc.2009.11.004

Mathias, S.A., Hardisty, P.E., Trudell, M.R., Zimmerman, R.W.: Approximate solutions for pressure buildup during CO_2 injection in brine aquifers. Transp. Porous Media **79**, 265–284 (2009c). doi:10.1007/s11242-008-9316-7

Nordbotten, J.M., Celia, M.A., Bachu, S.: Injection and storage of CO_2 in deep saline aquifers: analytic solution for CO_2 plume evolution during injection. Transp. Porous Media **58**, 339–360 (2005). doi:10.1007/s11242-004-0670-9

Pruess, K., Oldenburg, C.M., Moridis, G.: TOUGH2 user's guide, version 2.0. Report LBNL-43134, Lawrence Berkeley National Laboratory, Berkeley, CA, USA (1999)

Pruess, K.: ECO2N: A TOUGH2 fluid property module for mixtures of water, NaCl, and CO_2. Report LBNL-57952, Lawrence Berkeley National Laboratory, Berkeley, CA, USA (2005)

Rutqvist, J., Birkholzer, J.T., Tsang, C.F.: Coupled reservoir—geomechanical analysis of the potential for tensile and shear failure associated with CO_2 injection in multilayered reservoir—caprock systems. Int. J. Rock Mech. Min. Sci. **45**, 132–143 (2008). doi:10.1016/j.ijrmms.2007.04.006

Saripalli, P., McGrail, P.: Semi-analytical approaches to modeling deep well injection of CO_2 for geological sequestration. Energy Convers. Manag. **43**(2), 185–198 (2002)

van Genuchten, M.Th.: A closed form equation for predicting the hydraulic conductivity of unsaturated soils. Soil Sci. Soc. Am. J. **44**, 892–898 (1980)

Vilarrasa, V., Bolster, D., Dentz, M., Olivella, S., Carrera, J.: Effects of CO_2 compressibility on CO_2 storage in deep saline aquifers. Transp. Porous Media **85**, 619–639 (2010). doi:10.1007/s11242-010-9582-z

Welge, H.J.: A simplified method for computing oil recovery by gas or water drive. Trans. Am. Inst. Min. Metall. Pet. Eng. **195**, 91–98 (1952)

Yamamoto, H., Doughty, C.: Investigation of gridding effects for numerical simulations of CO_2 geologic sequestration. Int. J. Greenhouse Gas Control (2011). doi:10.1016/j.ijggc.2011.02.007

Zhou, Q., Birkholzer, J., Tsang, C., Rutqvist, J.: A method for quick assessment of CO_2 storage capacity in closed and semi-closed saline formations. Int. J. Greenhouse Gas Control **2**(4), 626–639 (2008)